Self-assembly of graphene oxide sheets: The key step toward highly efficient desalination

Lei Zhang[†,‖], Wen Li[*,†,‖], Mutian Zhang[†], Shougang Chen[*,†,]

† School of Materials Science & Engineering, Ocean University of China, Qingdao 266100 PR China

Corresponding author:

Shougang Chen E-mail address: oucsgchen@163.com

Wen Li E-mail address: wenli0720@gmail.com

‖ These authors contributed equally to this work.

DFT calculation for adsorption energies.

To eliminate the effect of multi-group interaction on the adsorption results, models containing hydroxyl, epoxy groups of graphene oxide clusters and graphene clusters were constructed, and their structures were optimized, respectively. Considering the charge attraction, the initial adsorption positions were selected as the top position. There were three adsorption sites for general surface adsorption: top site (Top), bridge site (Bridge), and hollow site (Hollow). During the process of structural optimization, some atoms adsorbed on top position (bridge) would migrate to Bridge site after the calculation accuracy was improved. As a result, we only selected the optimized adsorption site as the stable adsorption site.

Table S1. Calculation results of adsorption sites and adsorption energies between GO attached to different function groups or GN clusters with Na^+ and Cl^-.

Model	Eads（eV）	Adsorption distance	Adsorption atom	Position
GN-Na	-0.182507	2.532	C	Bridge
GN-Cl	-0.45326	3.359	C	Top
GO-COC-Na^+	-1.213438	2.450	O	Bridge
GO-COC-Cl^-	-2.476156	4.083	O	Bridge
GO-OH-Na^+	-0.772205	2.302	O	Top
GO-OH-Cl^-	-2.962233	2.190	H	Bridge

Detailed description of the water transport in NR-NR2 system.

The NR-NR2 model was similar to NR-NR channel (Figure 1a4). The interlayer distance of NR-NR2 channel was set as 0.75 nm, which was calculated by the interlayer distance of 9.3 Å subtracting the space occupied by functional groups of hydroxyl or epoxy (~1.8 Å). Apparently, although the effective interlayer spaces for water flow in the NR-NR2 and OR-OR systems are almost the same (~0.75 nm), water flow in the NR-NR2 system is much faster than that in the OR-OR system. This can be explained by the strong non-bonding interactions between the oxygen-containing groups and water molecules, including vdW, electrostatic interaction and H-bonds, which largely restrain the water transport. The results in Figure R2 further prove that the interactions between the oxygen-containing groups and water molecules play an important role in determining water transport.

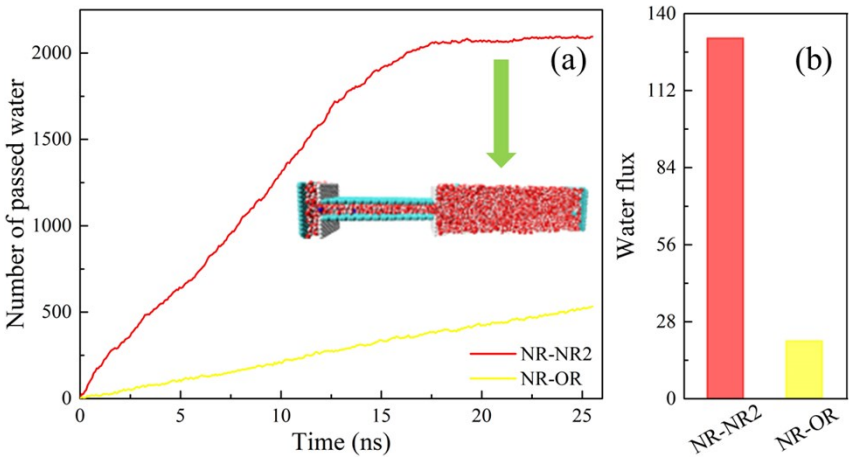

Figure S1. (a) Time evolution of the number of passed water molecules through NR-NR2 and NR-OR channels; (b) Water flux of the NR-NR2 and NR-OR channels. The inset in (a) shows the finial configuration when the number of passed water molecules reach a stable value.

Detailed description of the assembly process of the SGO sheets.

To describe the sliding processes of the SGO sheets (Figure 5b1-d1) quantitatively, Figure S1a-c show the time evolution of the geometric center of the SGO sheet along X, Y, and Z axes, respectively. For the SGO-R system, obvious motion of the SGO sheet in X and Y directions can be observed. However, for SGO-M and SGO-L systems, the motion of the SGO sheet is very slight, which is consist with the observed results in Figure 5. It can be concluded that the oxidation region of neighboring GO sheets is prone to match with each other as a result of the sliding of GO sheets in aqueous solution. For the movement of SGO sheet in Z direction (Figure S2c), its position always fluctuates in a limited region. Therefore, the averaged interlayer distances between the SGO and LGO sheets can be calculated (the carbon skeleton of the LGO sheet is fixed). The results show that the interlayer distances are 7.74, 7.84 and 7.53 Å for the SGO-L, SGO-M and SGO-R systems, respectively. It is obvious that these distances are larger than that of dried GO membrane. This is caused by the confined water molecules in the interlayer space of neighboring GO sheets.

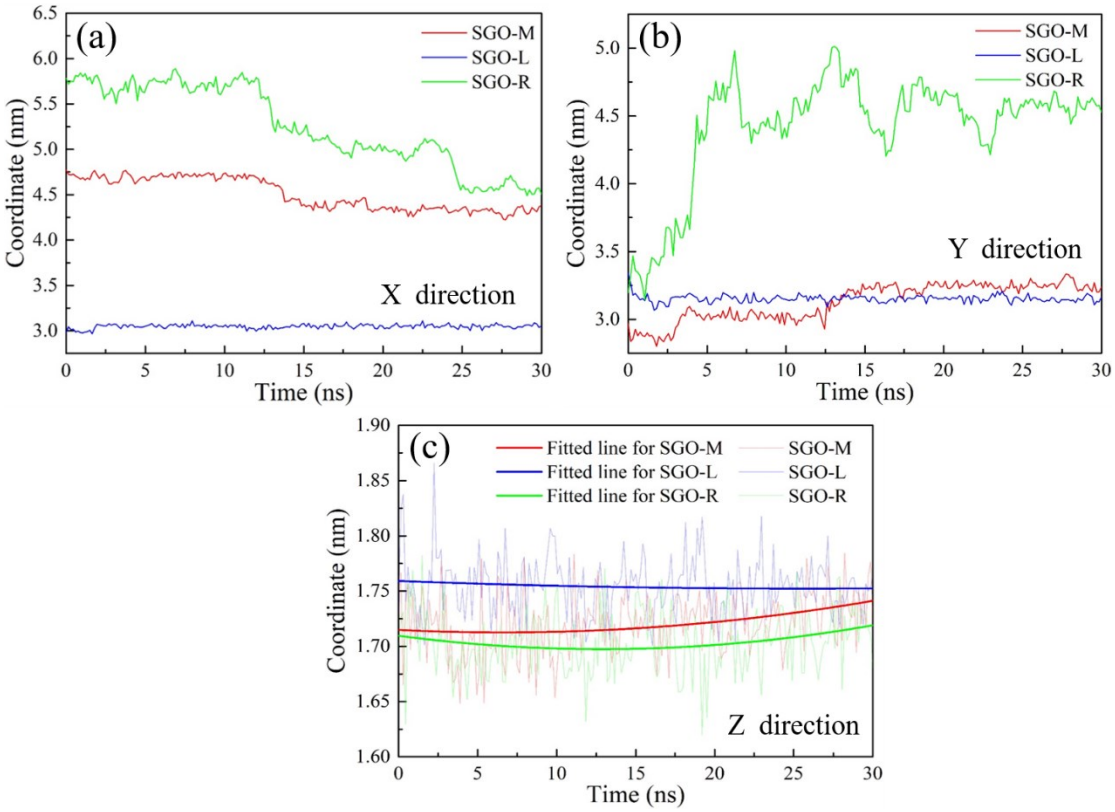

Figure S2. The coordinate changes of the geometric center of the SGO sheets in SGO-L, SGO-R, and SGO-R systems in (a) X, (b) Y, and (c) Z directions along with time.

Detailed description about the sliding and rotation process.

To describe the rotation of the SGO sheet quantitatively, the coordinate changes of the carbon atom located at the left upper corner of the SGO sheet are plotted in Figure S3a1-a3 for the SGO-M, SGO-L, and SGO-R systems, respectively. We can see that the coordinate changes are more obvious for the SGO sheet in SGO-R system followed by that of SGO-M and SGO-L systems. In addition, compared with Figure S2a and b, the coordinate changes of the carbon atom located at the left upper corner of the SGO sheet are more pronounced than that of the geometric center, implying the rotation of the SGO sheet during sliding. This is also confirmed by the snapshots of the dynamic trajectories of the simulation system (the insets in Figure S3a1-a3). In order to reveal the rotation and sliding processes more clearly, the coordinate changes of the atom at the left upper corner and the geometric center of the SGO sheet in X direction are drawn in Figure S3b1-b3. Accordingly, the whole assembling process of the SGO sheet can be divided into four, two, and six stages for the SGO-M, L, and R systems, respectively. Overall, at the first stage of the three systems, the coordinates of the atom at the left upper corner change a lot while the coordinates of the geometrical center change negligible. This indicates that the SGO sheet first experiences a rotating process without sliding.

For the SGO-M system, the two coordinates do not change on the whole at the second stage, indicating the Brownian motion of the SGO sheet at its original position. At the third stage (Figure S3b1), all the two coordinates decrease while the coordinates of the geometrical center decrease more obvious, indicating that the sliding and rotating of the SGO sheet are going on at the same time. In the fourth stage, the two coordinates fluctuate slightly, meaning that the system has reached a balanced stage. For the SGO-L system (Figure S3b2), the SGO sheet only rotates in its original position without obvious sliding because of the strong interfacial interactions between the SGO and the oxidation region of the LGO sheet. As for the SGO-R system (Figure S3b3), the first stage is a pure rotation process. The second and fourth stages belong to metastable states without obvious coordinate changes. At the third stage, the more obvious coordinate changes of the geometrical center than that of atom at the left upper corner indicate that the dominating process for the motion of the SGO sheet is sliding, and the rotation is weak. At the fifth stage, the both decreasing coordinates suggest that the sliding and rotating of the SGO sheet are going on at the same time. In contrast, the more obvious coordinate changes of the atom at the left upper corner indicates that the rotation of the SGO sheet is the dominate process. Finally, at the sixth stage, the system reaches a balanced state without obvious coordinate changes. Apparently, due to the rotation of the SGO-R at the first, third, and fifth stages, its rotation angel is the largest among the three studied systems (the insets in Figure S3a1-a3).

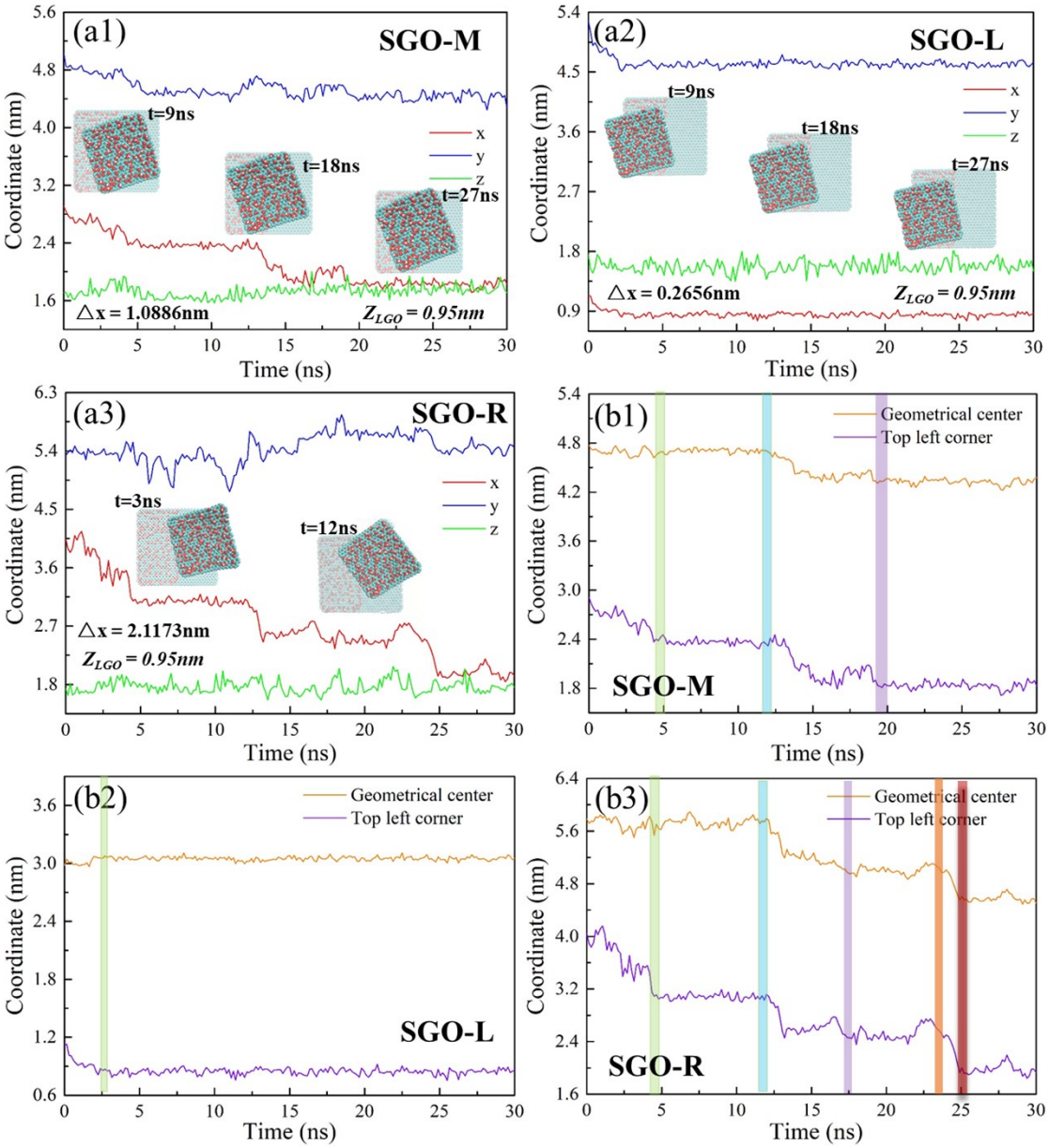

Figure S3. (a) Time evolutions of the coordinates of the atom located at the top left corner of the SGO sheet in (a1) SGO-M, (a2) SGO-L, and (a3) SGO-R systems. (b) Time evolutions of coordinates of geometric Center and the atom at the top left corner of the SGO sheet in (b1) SGO-M, (b2) SGO-L, and (b3) SGO-R systems. The insets in (a1-a3) present the conformation snapshots of the GO sheets at different time.

Theoretical analyses for the rotation mechanism of GO sheets.

In our analyses, the driving force for the sliding of the SGO sheet is considered to be identical no matter for directly sliding or sliding after rotation. For simplification, the rotation angle of 45° is chosen to make the process more intuitive. According to above discussion, the resisting force for the sliding of the SGO sheet is mainly from the non-bonding interactions between the SGO sheet and water molecules including electrostatic, vdW, and H-bonds interactions. As shown in Figure S4a1 and S4b1, before applying the driving force, the forces acting on the GO sheet from water molecules are balanced, and thus, generating the random movement of the GO sheet. Once a constant driving force is applied on the GO sheet, it will move forward. For direct sliding (Figure S4a1), the binding sites of water molecules at the front side will move forward, resulting in a shorter atomic distance. This will generate an interatomic non-bonding repulsive force to restrain the motion of the GO sheet. Analogously, the non-bonding force between the GO sheet and water molecule will also hinder the movement of the sheet (Figure S4a3). To obtain the resisting force for the motion of the GO sheet, we only focus on the horizontal component force parallel to the velocity direction, as shown in Figure S4c1 and c2.

Under static condition, the attractive and repulsive forces between water molecules and the GO sheet are equal, and we assume that the current distance between non-bonding atoms is 2a (a is positive constant, Figure S4a2). Once the GO sheet moves forward for a small distance of ka (0<k<2, Figure S4a2 and b2), the new atomic distance can be calculated by Cosine Law:

$$C^2 = A^2 + B^2 - 2AB\cos R \quad (1)$$

Where A is 2a, B is ka, and R is 90° for direct sliding of the GO sheet (Figure S4a2), and the R is 45° and 135° for the sliding of the GO sheet after rotating (Figure S4b2), respectively. Therefore, the new distances can be calculated and shown in Figure S4a2 and Figure S4b2 (purple numbers and symbols). For the nonbinding interactions, the attractive force will be the dominate interaction due to the increase of atomic distance, which can be calculated according to equation (2). Meanwhile, the repulsive force will be the dominate interaction due to the decrease of atomic distance, which can be calculated according to equation (3).

$$F_{att} = j / x_1 \quad (2)$$

$$F_{rep} = h / x_2 \quad (3)$$

Where x_1 and x_2 are the atomic distances between non-bonding atoms, F is the attractive (F_{att}) or repulsive force (F_{rep}) after sliding, and j and h are different coefficient of proportionality. As a result, the corresponding forces of F_1, F_2, F_3, F_4 and F_5 are calculated through the following equations (F_2, F_3, F_5 are the attractive forces and F_1, F_4 are the repulsive forces, Figure S4c1 and c2):

$$F_1 = j / (2-k)a \quad (4)$$

$$F_2 = h / (2+k)a \quad (5)$$

$$F_3 = h / (\sqrt{k^2 + 4}\, a) \quad (6)$$

$$F_4 = j / (\sqrt{k^2 + 4 - 2\sqrt{2}k}\, a) \quad (7)$$

$$F_5 = h / (\sqrt{k^2 + 4 + 2\sqrt{2}k}\, a) \quad (8)$$

In these equations, we only calculate the resisting force and ignore the force direction. Then, the component of each force in the direction parallel to the velocity direction of the GO sheet is calculated. Before that, some angles need to be firstly worked out, i.e. θ, α, and β in Figure S4c1 and c2. The angle in Figure S4c1 is calculated according to the geometric relation in Figure S4a2, which is conveyed by the equation:

$$\cos\theta = \frac{k}{\sqrt{k^2 + 4}} \quad (9)$$

As exhibited in Figure S4d1 and d2, the lengths of broadside can be worked out easily according to geometric relations. Therefore, the angles can be calculated by the following equation:

$$\sin\alpha = \frac{\sqrt{2} - k}{\sqrt{k^2 + 4 - 2\sqrt{2}k}} \quad (10)$$

$$\cos\beta = \frac{\sqrt{2} + k}{\sqrt{k^2 + 4 + 2\sqrt{2}k}} \quad (11)$$

Finally, the total resisting force when the GO sheet slides forward in the two situations can be calculated, in which the $F_{non\text{-}rotation}$ (the first situation) and $F_{rotation}$ (the second situation) are expressed by the equations:

$$F_{non\text{-}rotation} = F_1 + F_2 + 2 \times F_3 \cos\theta \quad (12)$$

$$F_{rotation} = 2 \times F_4 \sin\alpha + 2 \times F_5 \cos\beta \quad (13)$$

Where F_1, F_2, F_3, F_4, F_5, cosθ, sinα, and cos β have been calculated in equation (4), (5), (6), (7), (8), (9), (10) and (11), respectively. When $F_{non\text{-}rotation}$ is stronger than $F_{rotation}$, the following inequalities must be satisfied simultaneously due to the symmetry of the SGO sheets:

$$F_1 > 2 \times F_4 \sin\alpha \quad (14)$$

and

$$F_2 + 2 \times F_3 \cos\theta > 2 \times F_5 \cos\beta \quad (15)$$

To solve the inequalities, we firstly calculate F_1, $2\times F_4 \sin\alpha$, $F_2+2\times F_3\cos\theta$, and $2\times F_5 \cos\beta$ along with the changes of k, and the results are shown in Figure S5. We can obtained that the $F_{non\text{-}rotation}$ is stronger than $F_{rotation}$ when $0.615<k<2$ under the condition of $0<k<2$. We can also obtain that the differences between $F_{non\text{-}rotation}$ and $F_{rotation}$ are negligible when $0<k<0.615$, and the differences are quite obvious when $k>1.0$. In other words, the strength of $F_{non\text{-}rotation}$ and $F_{rotation}$ are almost the same when $0<k<0.615$, and the former one is always stronger than the latter one when $0.618<k<2$. Therefore, rotation of the SGO sheet is needed for the sliding of the SGO sheet to minimize the resistance. This also explains the small rotation angel when the SGO sheet is initially placed on the oxidized region of the LGO sheet due to its small driving force for sliding.

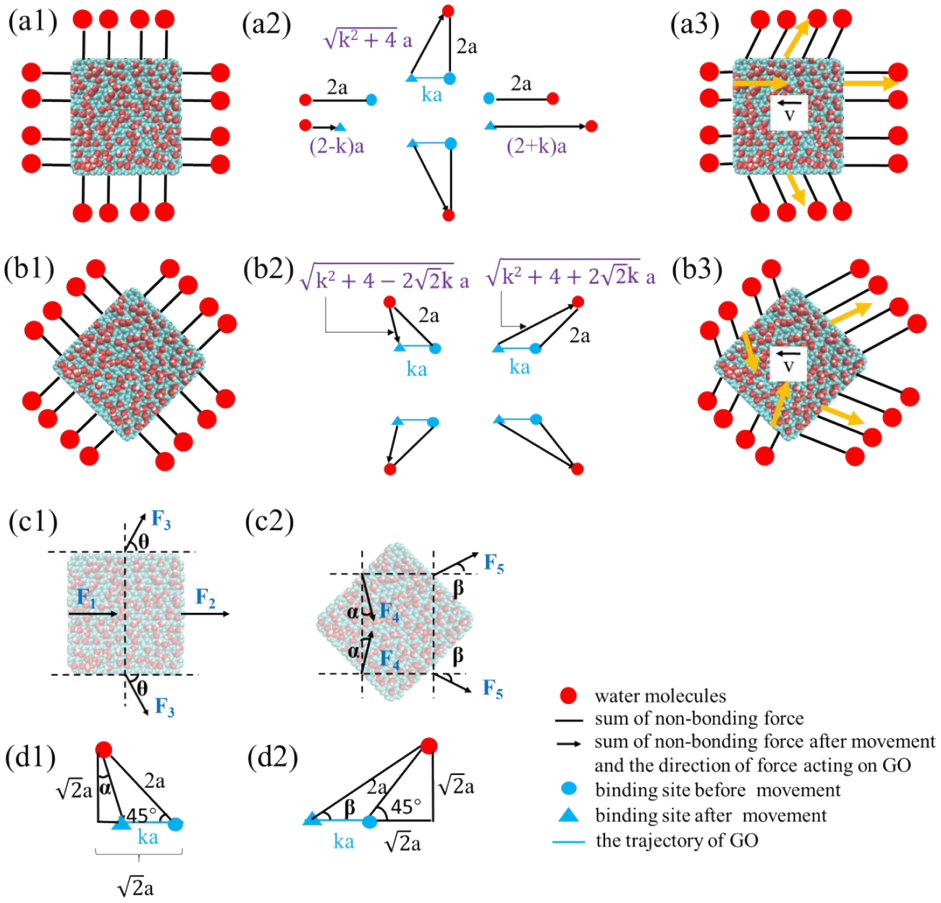

Figure S4. The schematic to calculate the resisting force for the movement of GO sheet under (a) direct sliding and (b) sliding after rotation; (c) Decomposition of the resisting force at each side of the GO sheet; (d1-d2) The configurations for the calculation of the lengths of sides. Resisting force of each side is marked with orange arrowheads in (a3) and (b3). The non-bonding interactions are signed by black lines to make the illustration clearer, and the black lines are not real bonds.

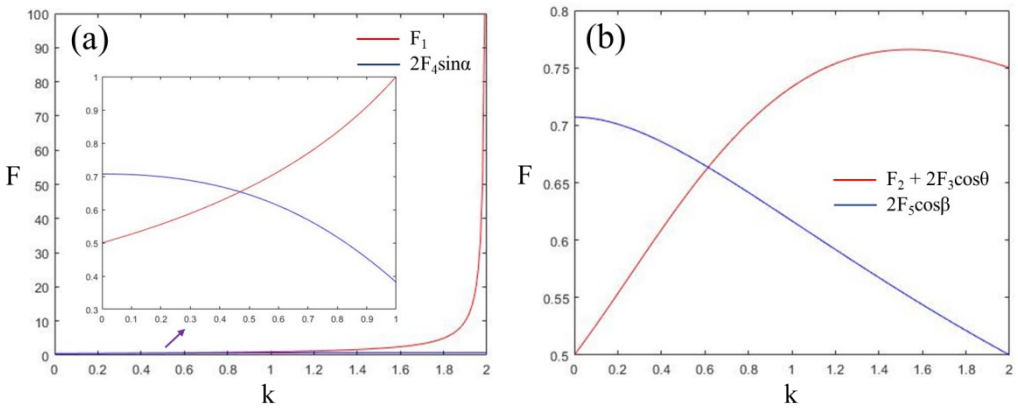

Figure S5. The evolution of the resisting force with the changes of k value.

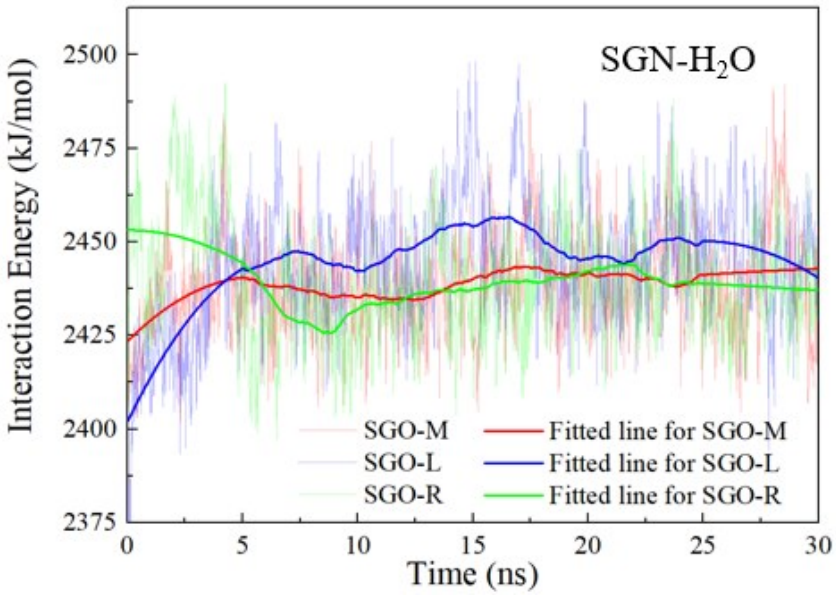

Figure S6. Time evolution of the interaction energies between the SGN sheet and water molecules.

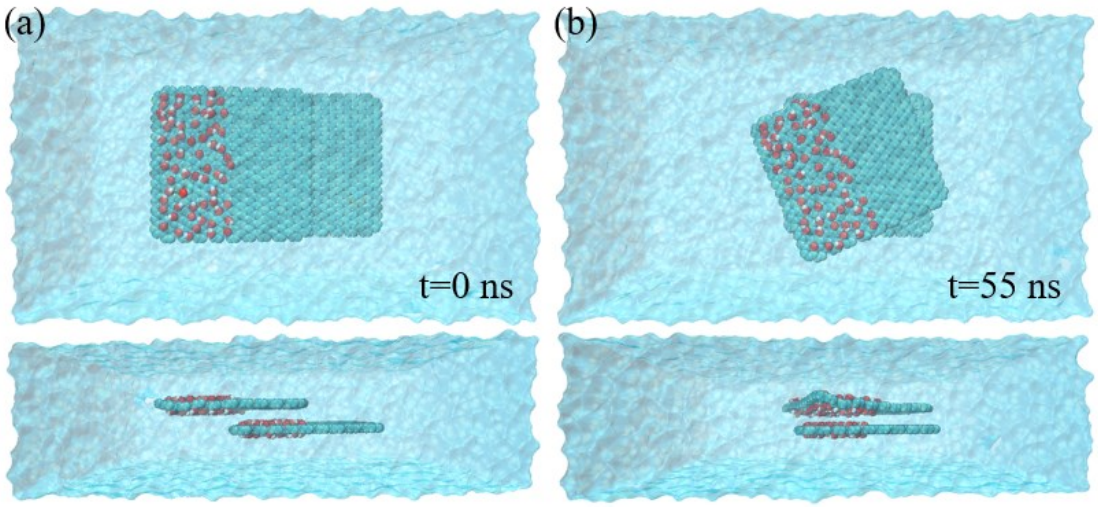

Figure S7. Top and side views of the long-time assembly of neighboring GO sheets.